Macromolecules
Article
Cite This: Macromolecules XXXX, XXX, XXX−XXX

Removal Pathways of Out-of-Plane Defects in Thin Films of Lamellar Forming Block Copolymers

Jun-Qing Song, Yi-Xin Liu,* and Hong-Dong Zhang

State Key Laboratory of Molecular Engineering of Polymers, Department of Macromolecular Science, Fudan University, Shanghai 200438, China

ABSTRACT: Understanding the defect removal process is crucial for fabricating defect-free self-assembled structures in block copolymer thin films. Most previous studies mainly focused on the removal of in-plane dislocation and disclination defects, while out-of-plane defects receive less attention. In this study, the removal of two types of out-of-plane defects of lamellar forming block copolymer thin films, the tilted domain defect and the cross-sectional edge dislocation defect, are studied in detail using the string method coupled with the numerical self-consistent field theory (SCFT). It is found that the removal of the tilted domain defect can be regarded as an order−order transition process controlled by the nucleation and growth mechanism. On the other hand, the cross-sectional edge dislocation can be eliminated by either evaporating or growing its core (a partial domain). For both cases, multiple removal pathways have been identified by varying the height of the partial domains and the segregation strength of the block copolymer. Phase-diagram-like maps are constructed to show which removal pathway can occur most probably at given height and segregation strength. In the strong segregation regime, in consistent with that found in the removal of in-plane defects, one or more "bridge" structures are formed, which serve as a channel for diffusion of polymer chains. When the segregation is weak, however, no actual bridge but only a nascent bridge structure, whose density of A components in the B domain is slightly higher than the averaging value, is observed and plays a similar role as the actual bridge.

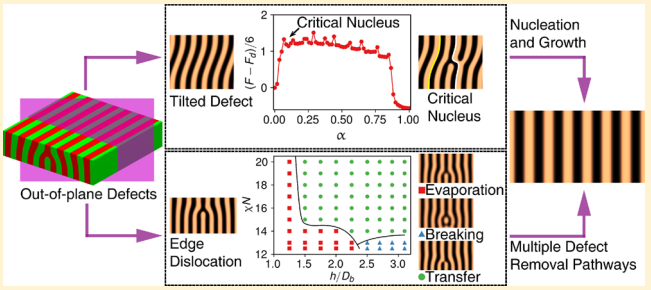

1. INTRODUCTION

Block copolymers in bulk can self-assemble into a variety of ordered nanostructures[1−7] owing to its long chain nature and the repulsion among dissimilar monomers. Polymer-related parameters, such as the chain architectures, the degree of polymerization, kinds of monomers, and Flory−Huggins interaction parameters, control the symmetry and periodicity of these nanostructures. By confining block copolymers in finite spaces, additional and more complicated nanostructures can be generated.[8,9] Furthermore, it is possible to precisely fabricate nanostructures with specific domain orientations by utilizing the fact that the symmetry breaks along confining directions. Among all confining systems, one-dimensional confinement, e.g., thin films, is of particular interest because of its potential applications in electronic devices,[10,11] nanolithography,[12] photovoltaics,[13,14] and porous membranes.[15]

In practice, thin films are fabricated by spin-coating[16] block copolymer solutions onto substrates followed by annealing. Domain orientations, either parallel or perpendicular to the substrate, can be controlled by optimizing the film thickness and tuning the surface property.[17−20] For example, directed self-assembly (DSA) on patterned surfaces using either chemoepitaxy[21−23] or graphoepitaxy[24,25] is an effective technique to prepare thin films with particular order. However, it is still challenging to prepare defect-free structures since the long-range order is easily destroyed by various in-plane and out-of-plane defects.[26,27]

In-plane defects, which appear in the top surface plane of the thin film, have been extensively studied through both theory[28−33] and experiment.[21,34−37] In the vicinity of the order−disorder transition(ODT), thermal fluctuations are the main cause for the occurrence of defectivity, while far away from the ODT, it is believed that defects are kinetically trapped metastable states.[38] In the thermodynamic aspect, in-plane defective structures usually have an excess free energy (ΔF_d) relative to the defect-free structures. Both self-consistent field calculations[28,31] and computer simulations[29,30] found that ΔF_d of a dislocation dipole is on the order of $100k_BT$, making it extremely difficult to form defects at equilibrium since the density of defects is expected to scale exponentially with the excess free energy as $n_d \sim \exp(-\Delta F_d/k_BT)$. It thus suggested that defects observed in experiments should arise in the kinetic process during the formation of microphase-separated structures. Once the defects exist in the system, in general it can only be removed through an activated process where a significant free energy barrier helps stabilize them.[29]

Kinetically, the diffusion of polymer chains plays an important role in removal of in-plane defects. Many experiments have studied the diffusion in microphase-separated structures, including lamellae,[39−44] cylinders,[45−47] spheres,[45,48]

Received: February 14, 2018
Revised: May 14, 2018

DOI: 10.1021/acs.macromol.8b00349
Macromolecules XXXX, XXX, XXX−XXX

and gyroids.[49] Generally, there are two diffusion modes:[48] one is the "interface diffusion" that polymer chains diffuse along the interface with their junctions positioned in the interface; the other is the "hopping diffusion" that polymer chains diffuse perpendicularly across the interface between two dissimilar domains. Generally, the diffusion coefficient of the hopping diffusion ($D_\perp$) is much smaller than that of the interface diffusion ($D_\parallel$) due to the enthalpic repulsion as polymer chains pass through the interface between dissimilar domains. The anisotropy of diffusion, $D_\parallel/D_\perp$, may depend on the length of polymer chains, the type of nanostructure, and the temperature. Tong and Sibener[34] obtained these diffusion coefficients by examining defect motions in cylinder-forming thin film. The interface diffusion occurs in climb motions of one dislocation pair, while the hopping diffusion appears in glide motions. The anisotropy of diffusion is found to be around 10 at high segregation strength. To avoid such slower hopping diffusion, it is found that the formation of a "bridge" structure is essential in the removal of in-plane defects. Taking the removal of the dislocation dipole as an example, a partial domain and one of its neighboring domains are first connected by forming a bridge structure. Then this bridge serves as a channel for polymer chains to conduct the inteface diffusion until the partial domain and the adjacent domain connect completely. Thus, the bridge provides an efficient way for transporting polymer chains to avoid the time-consuming hopping diffusion, especially when the anisotropy of diffusion is large.

Recently, out-of-plane defects are attracting more and more attention owing to the development of powerful characterization tools such as the grazing-incidence small-angle X-ray scattering (GISAXS)[27] and the sequential infiltration synthesis (SIS).[50] The tilted domain defect is a typical out-of-plane defect.[27,51] The mismatch between the periodicity of patterned substrates and lamellae is thought to be the main reason for the tilt of vertical domains, that these lamellar domains will relax from the constrained periodicity close to the patterned substrate to the bulk periodicity far away from it.[21,22,26,52,53] For uniform substrates, Mitra et al.[54] attribute the cause of tilted domains to the weak preference of the substrate: the preferred domains tend to increase the contact area with the substrate, leading to the formation of tilted domains. In addition, lamellar domains can tilt in response to the strain field near cross-sectional dislocations or disclinations,[55] and Vu et al.[56] found the tilted angle increasing with film thickness. Another example of out-of-plane defects, the cross-sectional edge dislocation, is topologically identical to the in-plane dislocation, in which a partial domain starts from the substrate but terminates in the middle of the thin film. Such defect is commonly observed in both perpendicular lamellae[24,26,57] and cylinders.[58] In summary, both tilted domain defect and the cross-sectional edge dislocation are widespread in experiments[24,26,56,58,59] and simulations[22,53,57] under various conditions. They can be observed in thin films of a wide range of film thickness[56] on either homogeneous,[54,56,59] patterned,[26,53] or rough[60,61] surfaces. Three-dimensional morphologies of these out-of-plane defective structures have been successfully revealed by computer simulations.[21,51] However, in contrast to the in-plane defects, the removal behavior of the out-of-plane defects has rarely been studied theoretically.

In this study, we explore extensively the removal of two out-of-plane defects, the tilted domain defect and the cross-sectional edge dislocation, in thin films of lamellae-forming diblock copolymers using the string method coupled with the numerical self-consistent field theory (SCFT). Two-dimensional simulations are performed, and both surfaces that confine the thin film are neutral and homogeneous. The article is organized as follows. First, the model and the numerical methods are briefly summarized. Next, the removal pathway of the tilted domain defect is examined carefully. The removal process can be regarded as an order−order transition, which is governed by the nucleation and growth mechanism. Then, multiple removal pathways are identified in the elimination of the cross-sectional edge dislocation. To remove the edge dislocation, the core of the edge dislocation can either shrink or grow. For both cases, a phase-diagram-like map in the plane of the initial height of the core of the edge dislocation and the segregation strength is constructed to show the most possible removal pathway under the corresponding condition.

2. NUMERICAL METHODS

2.1. String Method. The string method, developed by E et al.,[62,63] is a powerful tool to compute the minimum-energy paths (MEP) for complex, high-dimensional systems. The MEP, as a curve (string) in the configuration space connecting two local minima of a free energy landscape, corresponds to the most probable transition pathway between the two end states. It should satisfy the following condition[62,64]

$$(\nabla F)^\perp(\varphi) = 0 \tag{1}$$

where $(\nabla F)^\perp$ denotes the component of ∇F normal to the string φ parametrized by $\alpha \in [0, 1]$.

To compute the MEP, the string should first be initialized. There are many possible initialization schemes given that the two states at the string ends are known in prior. The nucleation-like initialization, which replaces a part of the starting state ($\alpha = 0$) with the corresponding part of the final state ($\alpha = 1$) to form intermediate states, is a natural choice for the study the nucleation process of first-order phase transitions.[64,65] Another initialization scheme, which constructs intermediate states by interpolating the two end states linearly with α as

$$\varphi(\alpha) = \varphi(0) + \frac{i}{M}[\varphi(1) - \varphi(0)] \quad i = 0, 1, ..., M \tag{2}$$

where $M + 1$ is the total states along the string, is appropriate for the study of the spinodal decomposition process of first-order phase transitions.[65] It is also widely used in finding possible pathways of the elimination of in-plane dislocations and disclinations.[28,29] In this study, both nucleation-like and linear-gradient initializations are used to explore the removal of the tilted domain defect, while the cross-sectional edge dislocation is studied using the linear-gradient initialization only.

After initialization, the string is relaxed using a two-step iterative procedure:[63] (i) updating the density distribution of each intermediate state along the string by applying a fixed number of SCFT iterations; (ii) interpolating and redistributing the new configuration uniformly on the string to avoid the collapse of the intermediate states to the local minima. An averaged energy, $\overline{F} = \sum_{i=0}^{M} F(\alpha_i)/(M + 1)$, is used to monitor the convergence of the update of the string. The MEP is then obtained when the difference of the averaged energy between two consecutive strings satisfies $\Delta\overline{F} = |\overline{F}_{i+1} - \overline{F}_i| < 10^{-6}$.

2.2. Self-Consistent Field Theory. We model the self-assembly of diblock copolymer (dBCP) under the thin film

DOI: 10.1021/acs.macromol.8b00349
Macromolecules XXXX, XXX, XXX−XXX

confinement by a numerical SCFT method. The top and bottom surfaces of the thin film are neutral and described by reflective boundary conditions, while the periodic boundary condition is applied in the lateral dimension. In this system of volume V, there are n symmetric dBCP chains composed of chemically incompatible components A and B with a Flory–Huggins parameter being χ. Each dBCP chain consists of N monomers with identical volume $v_0 = \rho_0^{-1}$ and length b. All spatial quantities are rescaled by the nonperturbed radius of gyration $R_g = b\sqrt{N/6}$. A compressible model by Helfand[66] is introduced to measure the penalty for local density fluctuations away from averaged density ρ_0, where its strength is characterized by a dimensionless parameter $\zeta > 0$

$$\beta U(r^{nN}) = \frac{\zeta}{2\rho_0}\int \mathrm{d}r[\sum_i \hat{\rho}_i(r) - \rho_0]^2 \tag{3}$$

In eq 3, ζ^{-1} is a measure of the compressibility of the model, so that the incompressible limit is approached as $\zeta \to \infty$. In this study, we set $\zeta N = 100$, which is large enough to accurately reproduce the phases and phase boundaries observed in incompressible model, and it dramatically speeds up the convergence of SCFT calculations.[67]

In the canonical ensemble, the partition function can be written as

$$Z = \mathcal{N}\int \mathcal{D}\phi_A \mathcal{D}\phi_B \mathcal{D}\omega_A \mathcal{D}\omega_B \exp(-H[\phi_i, \omega_i]) \tag{4}$$

The Hamiltonian, H, has the following form:

$$H/CV = \frac{1}{V}\int \mathrm{d}\mathbf{r}\Big[\chi N\phi_A\phi_B - \omega_A\phi_A - \omega_B\phi_B + \frac{\zeta N}{2}(\phi_A + \phi_B - 1)^2\Big] - \log Q[\omega_A, \omega_B] \tag{5}$$

where $C = \rho_0 R_g^d/N$ is a dimensionless constant and d is the dimension of space. Under the mean-field approximation, the partition function could be approximated as $Z \approx \exp(-F)$ where $F = H[\phi_i^*,\omega_i^*]/CV$ is the mean-field free energy. The dominant "mean-field" configurations ϕ_i^* and ω_i^* ($i = \{A, B\}$) are obtained by solving the saddle-point equations which results in a set of SCFT equations,

$$\omega_A N = \chi N\phi_B + \zeta N(\phi_A + \phi_B - 1)$$

$$\omega_B N = \chi N\phi_A + \zeta N(\phi_A + \phi_B - 1)$$

$$\phi_A = \int_0^{0.5} \mathrm{d}s\, q(\mathbf{r}, s; [\omega_A, \omega_B])q^*(\mathbf{r}, 1 - s; [\omega_A, \omega_B])$$

$$\phi_B = \int_{0.5}^{1} \mathrm{d}s\, q(\mathbf{r}, s; [\omega_A, \omega_B])q^*(\mathbf{r}, 1 - s; [\omega_A, \omega_B]) \tag{6}$$

Note that the superscript for the mean-field configuration is omitted. The propagator $q(\mathbf{r}, s; \omega)$ represents the probability for finding the s segment in a polymer chain at position $\mathbf{r}$ under the external field ω. The propagator can be solved from the Fokker–Planck equation

$$\frac{\partial q(\mathbf{r}, s; \omega)}{\partial \omega} = \nabla^2 q - \omega q \tag{7}$$

with the initial condition $q(\mathbf{r}, s = 0; \omega) = 1$. $q^*(\mathbf{r}, s; \omega)$ is a backward propagator which can be obtained similarly as $q(\mathbf{r}, s; \omega)$.[5]

The modified diffusion equations in SCFT are solved by a highly efficient fourth-order exponential time differencing Runge–Kutta method (ETDRK4) developed in our previous study.[68] The explicit Euler scheme is used to update the field configurations.[5] The Fourier spectral collocation are used in both the normal and the lateral directions of the substrate. The accuracy of free energy of single SCFT calculation is 10^{-5} or better with the spacing of grid points no larger than $0.2R_g$ and the time step along the chain contour is $\Delta s = 0.032$.

In this study, two-dimensional (2D) simulations are performed and all reported free energies are for 2D systems. Thus, the free energy of a 2D out-of-plane defect is typically one magnitude smaller than the reported free energies of three-dimensional (3D) defects. To obtain the free energy of a 3D out-of-plane defect, one can extrapolate the 2D results to 3D by assuming that the third dimension of the system is homogeneous and the free energy is linearly proportional to the size of the system.[28]

3. RESULTS AND DISCUSSION

3.1. Removal of the Tilted Domain Defect. *3.1.1. Nucleation and Growth Mechanism.* The tilted domain defect is commonly observed in perpendicular lamellae. The domain orientation obeys a Gaussian distribution with a standard deviation in the range of 8°–15° by analyzing GISAXS results.[27] Tilted domains are usually bent due to the deformation of thin films on weakly selective substrates. Sometimes, lamellar domains can tilt up to 40°.[54]

Here, we investigate a tilted domain defect where domains are both tilted and bent as depicted in Figure 1 ($\alpha = 0$). In the cross section, the thin film is composed of three parts: two

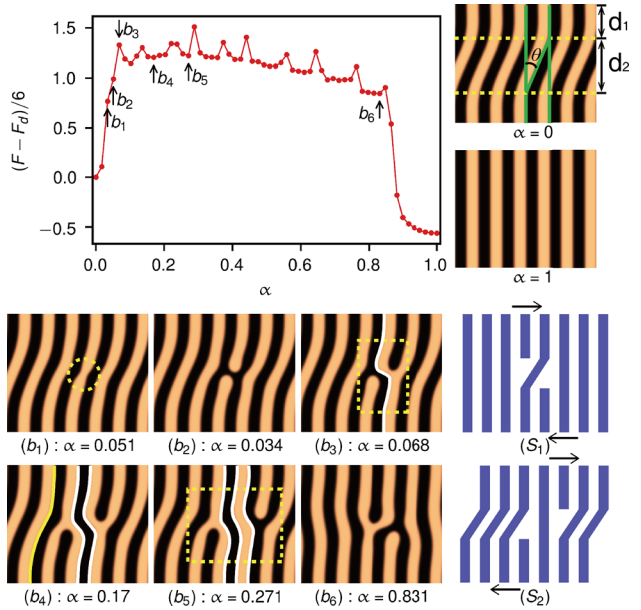

Figure 1. MEP between the tilted domain defect ($\alpha = 0$) and defect-free lamellae($\alpha = 1$) at $\chi N = 30$, $d_1 = 1.5D_b$, and $d_2 = 2D_b$. The abscissa represents the reaction coordinate along the pathway, $\alpha \in [0, 1]$. The vertical axis is the relative free energy per period between current state and the defective state ($\alpha = 0$) in units of k_BT. (b_1–b_6): morphological evolution along the string. The morphology in (b_6) has been shifted by three periods laterally. (S_1) and (S_2) demonstrate two modes of the glide motion of the dislocation pair. Bright and dark regions correspond to domains rich in A and B monomers, respectively.

DOI: 10.1021/acs.macromol.8b00349
Macromolecules XXXX, XXX, XXX–XXX

vertical parts near the top and bottom surfaces and one tilted part in the middle. The vertical parts have identical heights of $d_1 = 1.5D_b$, where D_b is the bulk lamellar period. The height of the tilted part is $d_2 = 2D_b$. The thickness of the thin film is $d = 2d_1 + d_2 = 5D_b$. In particular, we enforce the two vertical parts to align with each other as marked by the vertical green lines. The tilted domains skew for $1D_b$ in the lateral direction as shown by the slant green line. Correspondingly, the tilt angle is $\theta = \arctan(D_b/d_2) \simeq 26.57°$. Such kind of tilted domain defect is specially designed to overcome the difficulty on stabilizing the uniform tilted domains ($d_1 = 0$) on the neutral substrates during SCFT calculations. It is well-known that vertical lamellar domains are preferred on neutral substrates as both components of the block copolymer tend to wet the substrates equally.[69] Thus, the vertical parts in the tilted domains are employed to fulfill this condition. We have further verified that the use of the tilted domain defect with vanishing d_1 does not change the removal behavior significantly. In addition, similar tilted domain defect was observed in experiments.[60,61] However, unlike our system, in their studies rough substrates are used and the occurrence of the defect is suggested to be caused by processing procedures.

The out-of-plane tilted domain defect is different from the in-plane dislocations and disclinations.[29,30] In practice, in-plane defects and defect dipoles are point structures,[38] while the tilted domains can propagate in the lateral direction throughout the thin film.[54] Therefore, the tilted domain defect is a metastable structure with translational order similar to other ordered structures. On this basis, the process of the removal of the tilted domain defect to form perfect perpendicular lamellae could be treated as an order−order phase transition. Interestingly, the transition from tilted lamellae to perfect perpendicular lamellae seems to follow the nucleation and growth mechanism as shown in Figure 1, where the MEP connecting the tilted domain defect ($\alpha = 0$) and the defect-free lamellae ($\alpha = 1$) is presented. The nucleation begins with a random breakage of one of lamellar domains in the tilted part as shown in Figures 1(b_1) and 1(b_2). It is important to note that only one domain breaks up at a time, which is consistent with previous studies on the annihilation of the disclination.[28,34] The node (b_3) corresponds to the first transition state along the MEP, which is regarded as the critical nucleus. The critical nucleus, marked by the rectangular box in Figure 1(b_3), consists of one partial A domain, one partial B domain, one "bridge" connection, and one newly created AB interface. The "bridge" structure connects the top partial A domain and the adjacent whole A domain, which has also been observed in other studies.[28−31] The new AB interface marked by the white line indicates the formation of the defect-free lamella because the skew in the lateral direction is removed. The critical nucleus grows by propagating partial domains laterally, leaving the newly created whole domains behind. All transition states (peaks in the MEP) are associated with the formation of bridge structures. Meanwhile, more and more new AB interfaces marked by the white lines in (b_4) and (b_5) are generated. Because of the introduction of periodic boundaries in the lateral direction, the two partial domains will eventually encounter to form a dislocation dipole [(b_6)]. In practice, however, these two partial domains is unlike to encounter each other. The lateral propagation of partial domains can be trapped somewhere just like the glide motion of the in-plane dislocation dipole.[29] Two possible scenarios are the partial domain may become an isolated edge dislocation or it may encounter a partial domain created by another nucleation event to form a dislocation dipole.

In addition, one may notice that the free energy barrier (the height of the first peak (b_3) in Figure 1) corresponding to the formation of the critical nucleus, ΔF_b, is larger than the excess free energy of the tilted domain defect, $\Delta F_d = F(\alpha = 0) - F(\alpha = 1)$. In fact, ΔF_b is larger than ΔF_d for all χN in the range from 12.5 to 30 as shown in Figure 2. In consequence, it should be

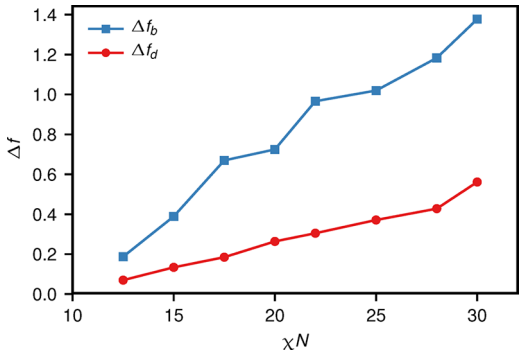

Figure 2. Excess energy of the tilted domain defect $\Delta f_d = \Delta F_d/6 = [F(\alpha = 0) - F(\alpha = 1)]/6$ and the energy barrier Δf_b as functions of χN.

easier for thermal fluctuations to create the tilted domain defect than to remove it. This result explains why the tilted domain defect is widely observed in experiments. Moreover, we also expect that the solvent[57] or thermal[70] annealing which facilitates the removal of in-plane defects by reducing the effective segregation strength is no longer an effective way to remove the tilted domain defect. Note that the result in Figure 2 is consistent with past self-consistent field simulations[28,31] and particle-based simulations[29] of in-plane defects that both ΔF_b and ΔF_d decrease almost linearly with χN. However, the relative position of the ΔF_b and ΔF_d curves is reversed.

In calculation of the result in Figure 1, the string is initialized by a linear-gradient scheme, while previous studies on the nucleation process utilized a nucleation-like initialization.[64,65,71] To verify our results, nucleation-like initialization is also implemented to search possible transition pathways in the removal of the tilted domain defect. The initial string is defined as $\phi(\alpha, \mathbf{r}) = \phi(1, \mathbf{r})$ if $\mathbf{r} \in \{\mathcal{B}_\alpha\}$, and $\phi(\alpha,\mathbf{r}) = \phi(0,\mathbf{r})$ otherwise, so that the domain, $\mathcal{B}_\alpha$, is filled with defect-free lamellae ($\alpha = 1$) while its outside is occupied by tilted domains ($\alpha = 0$). $\mathcal{B}_\alpha$ is a sequence of rectangles as shown in the sketch in Figure 3. The height of each rectangle is the same as the thickness of the film, while their width increases linearly with the string parameter α. As expected, the resulted MEP in Figure 3 is almost identical to that presented in Figure 1.

We have also examined the case when tilted domains skew for $2D_b$ in the lateral direction, and the result is given in Figure 4. It is found that this tilted domain defect can be decomposed into two parts separated by the yellow dashed line (see the inset image). For each part, the tilted domains skew for only one period and only one tilted domain randomly breaks up just like Figure 1. So there are two breakages as shown in Figures 4(b_1) and 4(b_3) corresponding to two largest energy barriers along the MEP. A complex critical nucleus is then generated after these two breakages enclosed by the rectangular box with yellow border lines in Figure 4(b_4), which is composed of three partial A domains, one partial B domains, one bridge structure,

DOI: 10.1021/acs.macromol.8b00349
Macromolecules XXXX, XXX, XXX−XXX

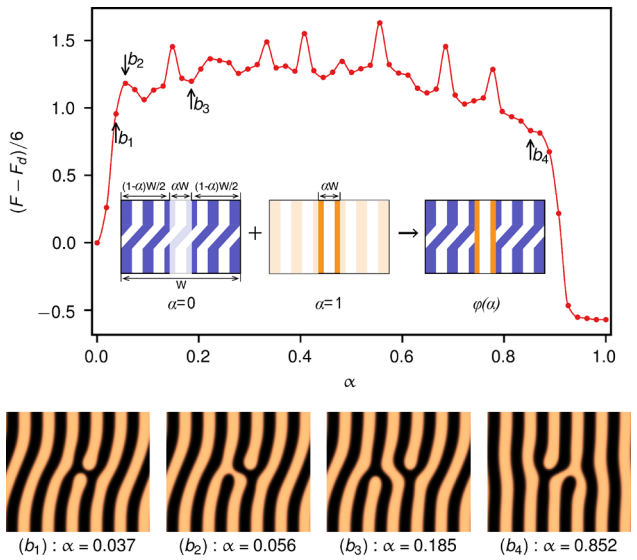

Figure 3. MEP at χN = 30 when the string is initialized in a nucleation-like manner. Other parameters are the same as Figure 1.

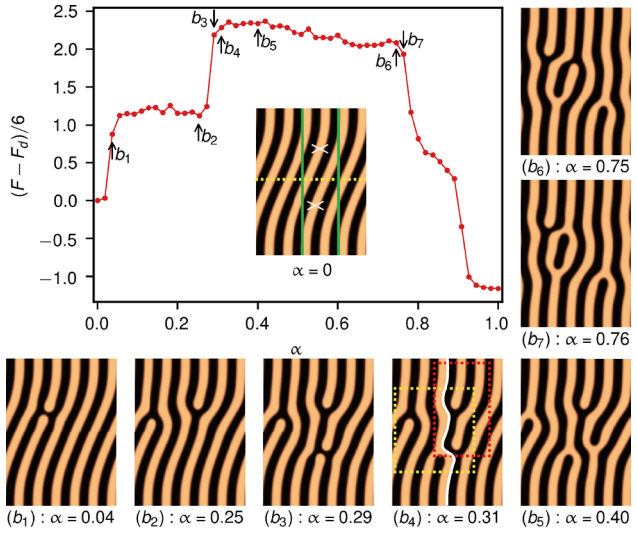

Figure 4. MEP at χN = 30 when the tilted layers skew for two periods in the lateral direction with $d_1 = 2D_b$ and $d_2 = 4D_b$. The morphologies in (b_6) and (b_7) have been shifted for $3D_b$ in the lateral direction to facilitate observation.

and one straight AB interface without any lateral skew (marked by the white line). Then this nucleus grows through the lateral propagation of the four partial layers. Meanwhile, more straight AB interfaces are created. Clearly, the shape and the growth of the critical nucleus depend on the degree of tilt of the tilted domain defect. The number of breakages of domains is the same as the number of periods that the tilted domain skews.

3.1.2. Sources for the Formation of Out-of-Plane Defects. To devise effective strategies for fabricating defect-free structures, it is crucial to understand and control the thermodynamics and dynamics of the defects. As mentioned in the Introduction, defects in thin films can be either generated by thermal fluctuations near the ODT or trapped as metastable states along the kinetic pathway of an order−disorder/order−order transition. In this study, it is found that the removal of one type of defect is an additional source for the formation of other types of defects. The first example is the defect shown in Figure 1(b_2) where one whole A domain is broken into two partial domains. This kind of defect is actually the "discrete" domain defect observed in cylinder-forming thin films.[24,72−74] While random nucleation at the top and bottom surface is a possible source for this disconnection defect,[74] our calculations reveal another possibility. The second example is the cross-sectional edge dislocation shown in in Figure 1(b_4) which is a metastable state during the removal process of the tilted domain defect. This defect was reported to exist in both lamellar-forming thin films[24,26,57,75] and cylinder-forming thin films.[58] The third example is the occurrence of two edge dislocations with the same sign of the Burger's vector marked by the rectangle with red border lines in Figure 4(b_4). This structure is exactly the same as experiment results.[26] The final example is the formation of an isolated droplet (or two opposing dislocations) as shown in Figure 4(b_7). The removal of this defect has been systematically studied by Li and co-workers.[31,32]

Actually, the source has also been revealed by previous simulation works. For example, the glide motion of the in-plane dislocation dipoles separated by multiple domains can produce dislocation dipoles with different intervals.[29] The MEP of this defect removal pathway consists of a series of metastable states corresponding to various defective structures. Similarly, the tight dislocation dipole is found to be resulted from the climb motion of two separated dislocations,[32,34] or it is a metastable state during the removal of disclinations.[28,34,76] Another example is three-dimensional (3D) DSA dislocation defects[29] that at the top surface it is a typical edge dislocation while at the bottom surface it is partially cured by a bridge structure. This 3D defect is a long-lasting metastable state in the removal process of dislocation dipoles.

3.1.3. Interactions between Edge Dislocations. The edge dislocation in lamellae can be characterized by Burgers vector.[77] Generally, two dislocations with same Burgers vectors are repulsive and tend to align in a row successively. One of examples of this alignment can be seen in Figure 4(b_4) indicated by the rectangular box with red dashed border lines.

Two dislocations with opposite Burgers vectors are attractive and can merge into one whole domain.[26] The attraction can be described by a distortion-mediated Peach−Koehle force which is proportional to the reciprocal of the interval between two opposing dislocations.[32] Both in-plane tight dislocation dipoles[28,30,31] and separated dislocation dipoles[29] share a common topological structure as shown in Figure 1(S_1) where partial domains are separated by tilted domains and surrounded by straight domains. The partial domains tend to propagate toward each other to remove the distorted interfaces to reduce the interfacial energy. In this study, it is found that out-of-plane dislocation dipoles with opposite Burgers vectors can be repulsive instead of attractive by exchanging the tilted and straight domains as shown in Figure 1(S_2). In this case, the thermodynamic driving force will drive the two partial domains propagating in opposite direction as shown in Figures 1(b_3), 1(b_4), and 1(b_5). Therefore, whether the interaction between two dislocations in a dipole is attractive or repulsive will depend on its topological structure.

3.2. Removal of the Cross-Sectional Edge Dislocation.

The cross-sectional edge dislocation is another typical out-of-plane defect in both the lamellar-forming and cylinder-forming thin films.[21,24,53,55,57,58,75] In section 3.1, we propose that the removal of the tilted domain defect is a possible source for producing this defect. Typical two-dimensional (2D) morphol-

DOI: 10.1021/acs.macromol.8b00349
Macromolecules XXXX, XXX, XXX−XXX

ogies of this defect in the cross section of a lamellar-forming thin film are presented in Figures 5(*b*) and 5(*c*), where a partial

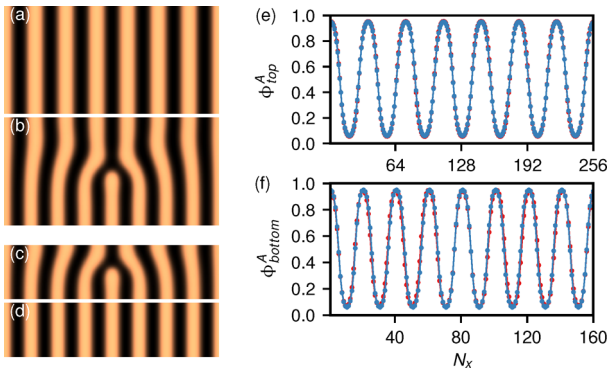

Figure 5. Morphologies of the defective structures and the defect-free lamellae for (a, b) the partial domain evaporates and for (c, d) the partial domain grows at $\chi N = 15$. The defective lamellae and defect-free lamellae are forced to align maximally. The density distributions of A block at top surface of (a) and (b) and at bottom surface of (c) and (d) are plotted in (e) and (f), respectively.

domain is symmetrically surrounded by a sequence of tilted domains. In practice, the cross-sectional edge dislocation is sometimes an isolated defect,[55] while in our calculations the defect can be considered as a dislocation dipole due to the use of periodic boundary conditions in the lateral direction. Therefore, to minimize the interactions between the two dislocations of the dipole, the width of the simulation cell should be chosen as large as possible. In this study, the width of the simulation cell is taken to be 7 or 8 bulk lamellar periods which has been verified to be large enough by comparing the results with simulations performed in a 22 bulk lamellar period cell. During the removal of the edge dislocation, the partial domain may either evaporate or grow. Correspondingly, the defect-free lamella should contain either 7 or 8 bulk periods in the simulation cell, as shown in Figures 5(*a*) and 5(*d*), respectively. In both cases, multiple removal pathways are discovered by varying the height of the partial domain and the segregation strength.

The width of the simulation cell for the defect structure ($\alpha = 0$) is determined by using a similar approach proposed by Li and Müller.[32] To ensure that the domains near the top surface (7 periods) and near the bottom surface (8 periods) are equally frustrated, the width of the simulation cell is given by

$$L = (N_p + \epsilon)D_b$$

$$\epsilon = \frac{\tau}{1+\tau}$$

$$\tau = \sqrt{\frac{N_p h}{(N_p+1)(d-h)}} \tag{8}$$

where $N_p = 7$, d is the thickness of the thin film, and h is the height of the partial domain. Then the width of the simulation cell for each intermediate states of the string is linearly interpolated between those at the two ends, i.e., $W_\alpha = (1-\alpha)W_0 + \alpha W_1$ with W_α, W_0, and W_1 being the widths of the simulation cells at α, $\alpha = 0$, and $\alpha = 1$, respectively. Consequently, the number of polymer chains in each simulation cell along the string is different because the volume of the simulation cell changes while the monomer density is kept as a constant. In other words, the system is not conserved along the string and polymer chains are free to flow in and out of the simulation cell. In addition, the defective lamellae at $\alpha = 0$ and the defect-free lamellae at $\alpha = 1$ are forced to align maximally. To see that the density distribution of A monomers at the top surface (when the defect-free lamella contains 7 periods) and the bottom surface (when the defect-free lamella contains 8 periods) are plotted in Figures 5e and 5f, respectively. In the following, we will explore the possible removal pathways of such kind of the cross-sectional edge dislocation.

3.2.1. Shrinking of the Partial Domain. One of the major advantages of the string method is its ability to explore multiple MEPs for the order−order transition.[28,64,65] Here, three distinct removal pathways are revealed by the string method when the partial domain in the edge dislocation choose to evaporate and eventually diminish. When the height of the partial domain is small and χN is low, it tends to shrink continuously during the removal process as shown in Figure 6(a_1−a_4). This pathway is

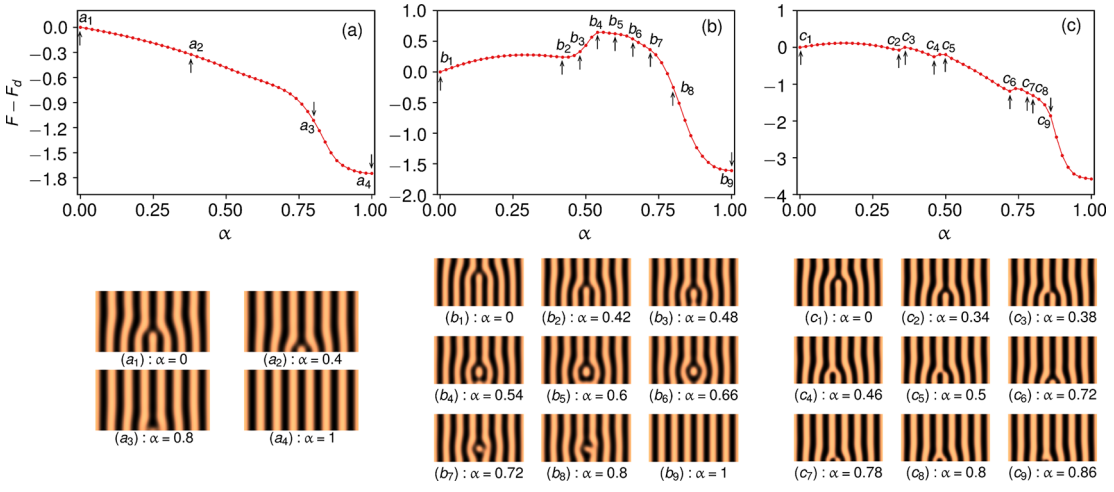

Figure 6. Three possible removal pathways of the cross-sectional edge dislocation when the core of the defect shrinks and eventually diminishes: (a) the evaporation pathway at $h = 1.25D_b$ and $\chi N = 12.5$; (b) the breaking pathway at $h = 2.7D_b$ and $\chi N = 12.5$; and (c) the transfer pathway at $h = 2.25D_b$ and $\chi N = 15.0$. The bright domains are rich in A monomers.

DOI: 10.1021/acs.macromol.8b00349
Macromolecules XXXX, XXX, XXX−XXX

named as the evaporation pathway. The corresponding MEP is plotted in Figure 6a. This pathway is similar to the evaporation mechanism of the elimination of the isolated droplet between two opposing in-plane dislocations reported by Li and co-workers.[31,32] In their system, the free energy in the MEP decreases linearly with the size of the droplet. The authors speculated that the evaporation of the droplet is driven by a constant boundary-induced force. In our system, the free energy curve loses linearity because the boundary-induced force is released due to the linear variation of the width of the simulation cell. Instead, the evaporation of the partial domain is solely driven by the thermal driving force.

According to the observations in section 3.1, the transportation of polymer chains is facilitated through a bridge connection that is always associated with a transition state in the MEP. In the evaporation pathway, however, there is no transition state along the MEP. It is thus interesting to show how polymer chains diffuse during the removal of the partial domain. In Figure 6a, we see that there is indeed no bridge connection formed during the removal process as expected. By zooming in the core of the edge dislocation, its typical morphology (α = 0.2) is shown in Figure 7a. We noticed that the region in the B domain depicted by the oblique line is slightly brighter than other regions of the B domain. To see it more clearly, we plot the density distribution of A monomers along the oblique line in Figure 7a. The density distribution of A monomers along the horizontal line is plotted as well to serve as a reference. It can be seen that the lowest density of A monomers along the oblique line is about twice higher than that along the horizontal line. Such relatively higher density region of A monomers in the B domain is reminiscent of the bridge structure, which we will call it the "nascent bridge" structure throughout this paper. Therefore, it is reasonable to assume that the diffusion of polymer chains from the partial domain to the adjacent A domains is mainly through the nascent bridge. Furthermore, it is known that the coefficient of the hopping diffusion is comparable to that of the interface diffusion at low χN.[46] Thus, it is not necessary to create actual bridge structures to facilitate the diffusion of polymer chains via the interface diffusion. This may explain why there is no actual bridge structure formed along the evaporation pathway. By increasing the segregation strength as shown in Figures 7b and 7c, however, the difference of the density of A monomers in the B domain along the oblique and the horizontal lines vanishes, indicating that the nascent bridge is hard to form at high χN. Consequently, we expect that the actual bridge instead of the nascent bridge will eventually form in the strong segregation regime, which leads to other removal pathways we will discuss next.

When the height of the partial domain is large enough and χN is small, the removal of the edge dislocation follows another pathway which we called it the breaking pathway. The MEP of this pathway and the corresponding morphologies at $h = 2.7D_b$ and χN = 12.5 are shown in Figure 6b. In this pathway, the partial domain first shrinks in a way similar to the evaporation pathway [see Figures 6(b_1), 6(b_2), and 6(b_3)]. However, the free energy in the MEP gradually increases when $\alpha < 0.3$ and other than that decreases in the evaporation pathway. The bottom part of the partial domain narrows as it shrinks. Eventually it will break apart at the neck to form a droplet as shown in Figure 6(b_4). The breaking of the partial domain is associated with a free energy barrier on the order of $1k_BT$. Note that the formation of the droplet should increase the AB interface area. Consequently, it will accelerate the removal of partial A domains to reduce the unfavorable AB interfaces. Moreover, we also observe four nascent bridge structures which are similar to that found in the evaporation pathway. Unlike the removal of a droplet by the evaporation mechanism,[31] here the droplet will be removed via an actual bridge connection formed at α = 0.72 [see Figure 6(b_7)]. It is worth noting that the merging of the droplet with the adjacent A domain has also been observed in the experiment.[47]

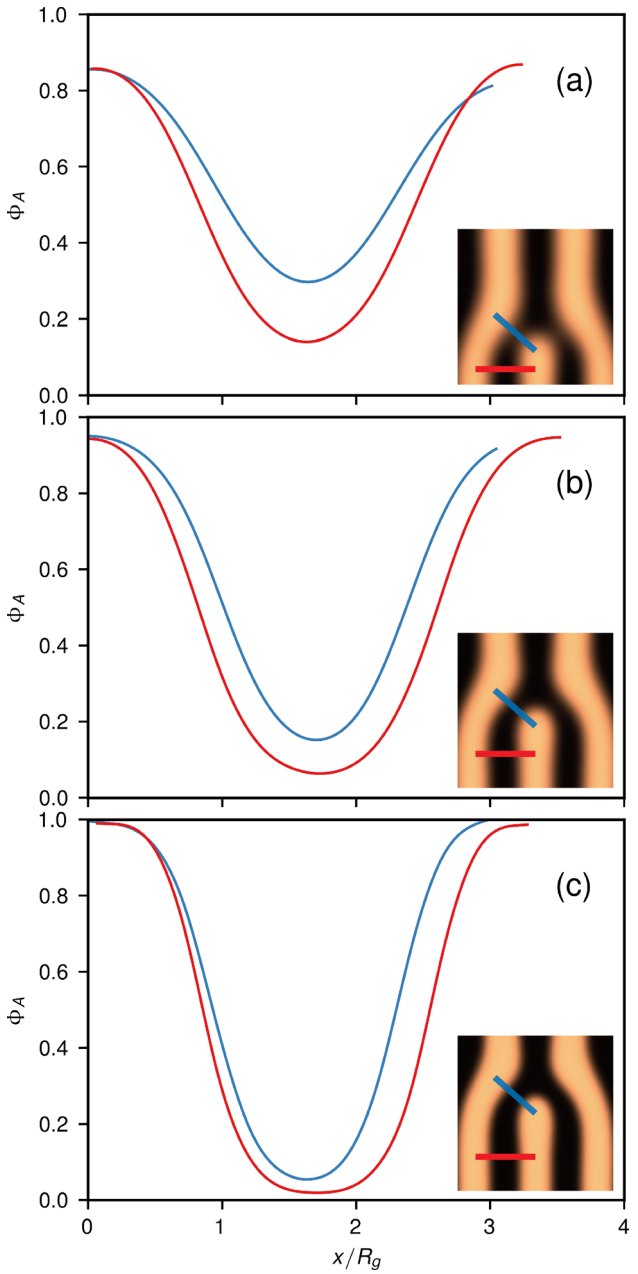

Figure 7. Morphologies of the cross-sectional edge dislocation and density distributions along the marked lines at (a) χN = 12.5, (b) χN = 15, and (c) χN = 20.

As χN increases, the cross-sectional edge dislocation is eliminated through a third pathway which we called it the transfer pathway. The MEP of this pathway and its associated morphologies at $h = 2.25D_b$ and χN = 15 are presented in Figure 6c. Along this pathway, two A bridges and one B bridge are formed at α = 0.38, 0.78, and 0.5, respectively. After the first

DOI: 10.1021/acs.macromol.8b00349
Macromolecules XXXX, XXX, XXX−XXX

A bridge is completely developed, the branched B domain that encloses the partial A domain is broken apart. As a result, the edge dislocation with a partial A domain as its core is transferred to an edge dislocation with a B core at $\alpha = 0.46$. The B core edge dislocation is then transferred to A core edge dislocation by formation and completion of a B bridge. The transfer of the core of the edge dislocation is accompanied by the decrease of the height of the core until the complete vanishing of the core. The alternation between A core and B core edge dislocations is actually observed in experiments as reported by Tsarkova and co-workers.[47]

The strong segregation strength is essential for the occurrence of the transfer pathway which can be explained as follows. On the one hand, the surface energy of the AB interface increases with χN, which means the partial domain becomes harder to be broken apart at high χN, making the breaking pathway unlikely to occur. On the other hand, the hopping diffusion for polymer chains in the partial A (or B) domain passing through the B (or A) domain to the adjacent A (or B) domain is more and more retarded as χN increases due to the strengthening of the enthalpic repulsion between A and B monomers. To avoid such slow hopping diffusion, it is preferred to convert it into the interface diffusion by creating a bridge that connects the partial domain and its adjacent domain. Note that only one bridge is formed at a time, although there are two potential locations suitable for formation of the bridge owing to the mirror symmetry of the edge dislocation. The reason is that the formation of the bridge is always associated with an energy barrier, and this energy barrier should be doubled when two bridges are formed simultaneously, as confirmed by the simulation works on the removal of the disclination defect by Takahashi and co-workers.[28]

In summary, the cross-sectional edge dislocation can be removed via multiple pathways under various conditions. At low χN, the transportation of polymer chains between the core of the edge dislocation and its neighboring domain is mainly completed by the hopping diffusion along a nascent bridge structure, while at large χN, the interface diffusion replaces the hopping diffusion by establishing a bridge. At low χN, the actual bridge is never formed and two pathways are possible depending on the height of the core of the edge dislocation. The evaporation pathway appears at low χN and small h, while the breaking pathway tends to occur at low χN and large h. The transfer pathway happens at large χN for a wide range of h. All above results are summarized in a phase-diagram-like plot in the $\chi N \sim h$ plane as shown in Figure 8. It should be noted that the map of different pathways only reflects the most possible kinetic pathway at corresponding parameters. We expect that in practice other pathways other than that is designated in the map might also be observed.

3.2.2. Growth of the Partial Domain. Similar to the case of shrinking of the partial domain during the removal of the cross-sectional edge dislocation, multiple removal pathways are also identified when the partial domain chooses to grow rather than to shrink. In the weak segregation regime ($\chi N \leq 14$), a direct growth pathway occurs where the partial domain continuously grows until it touches the top surface and forms a complete A domain. A typical MEP of this pathway together with its morphological sequence at $\chi N = 12.5$, $h_c = 0.64D_b$, and $d = 2D_b$ is presented in Figure 9a. Note that here we define a complementary height of the partial domain (h_c) instead of its height (h) as $h_c = d - h$. Hence, the smaller the value of h_c,

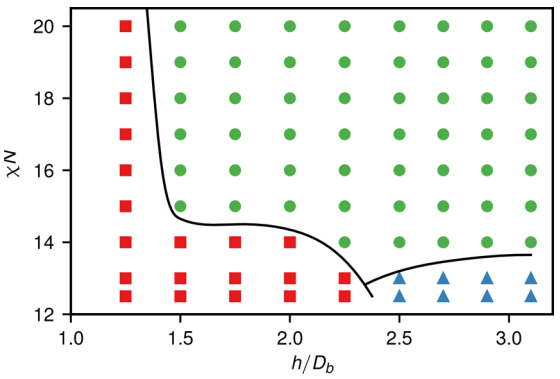

Figure 8. Possible removal pathways of the cross-sectional edge dislocation in the $\chi N \sim h$ plane when its core shrinks and eventually diminishes. h is the initial height of the core of the edge dislocation. Red squares: the evaporation pathway; blue up triangles: the breaking pathway; green solid circles: the transfer pathway. The thin film thickness is $4D_b$.

the higher the possibility that the partial domain tends to grow rather than shrink. It can be seen that the MEP decreases monotonically without any barrier or shoulders, meaning that there is no transition state along the pathway, which is similar to the evaporation pathway mentioned previously. Another common point between the direct growth pathway and the evaporation pathway is that they both rely on the nascent bridge structure to conduct the hopping diffusion of polymer chains between two A domains separated by a B domain. Two nascent bridge structures are marked by two oblique lines in the inset of Figure 9a, which can be compared with Figure 7a.

In the relatively strong segregation regime ($\chi N > 14$), when h_c is small, the cross-sectional edge dislocation is removed according to the top-bridge pathway. Figure 9b shows a typical MEP and a sequence of morphologies along the pathway at $\chi N = 18.0$ and $h_c = 0.85D_b$. There are two barriers in the MEP which correspond to the formation of the bridge at the top surface ($\alpha = 0.24$) and the breaking of the top bridge ($\alpha = 0.56$). Before the first barrier, the partial domain grows in a similar way as the direct growth pathway. Further growth of the partial domain leads to the formation of a bridge at the top surface at $\alpha = 0.24$. Note that its associated free energy barrier is significantly lower than the second barrier, which is understood that the enthalpic repulsion is weaker where there is a foreign surface.[29] Following that, the bridge thickens to form a parallel domain, which turns the cross-sectional edge dislocation into a disclination ($s = +1/2$)[26] at $\alpha = 0.5$. This disclination has been observed in experimental works.[24,28] The disclination is then eliminated by breaking the top bridge at right corner and a Γ-like structure is formed consequently at $\alpha = 0.56$. The broken bridge and the partial domain merge together via another bridge at $\alpha = 0.62$, where a shoulder rather than a barrier is associated with this process in the MEP. As a consequence, the original A core edge dislocation is transformed into a B core edge dislocation. Finally, the B core edge dislocation is removed via a similar pathway as the direct growth pathway.

By decreasing the height of the core of the edge dislocation in the relatively strong segregation regime, the removal of the edge dislocation follows a middle-bridge pathway. A typical MEP of this pathway and its associated morphologies at $\chi N = 19.0$ and $h_c = 1.22D_b$ are given in Figure 9c. The main feature of this pathway is that a bridge is formed in the middle of the film

DOI: 10.1021/acs.macromol.8b00349
Macromolecules XXXX, XXX, XXX−XXX

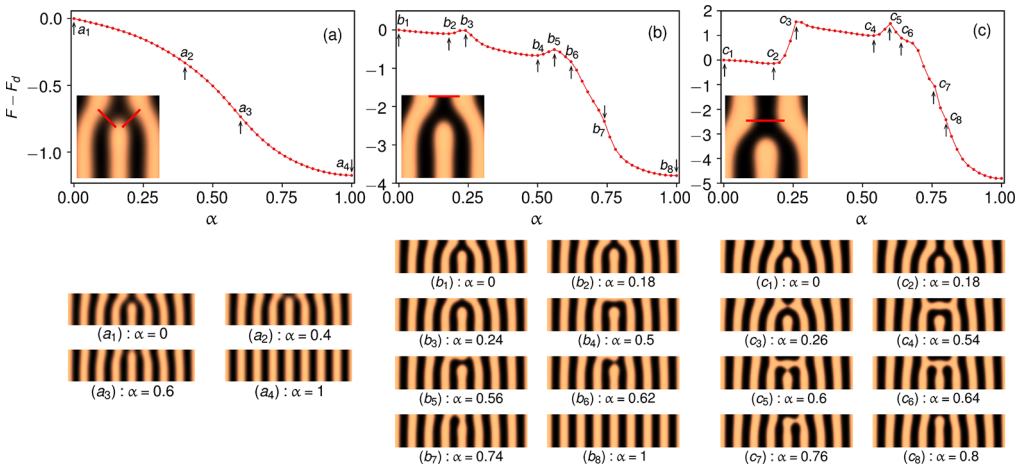

Figure 9. Three possible removal pathways of the cross-sectional edge dislocation when the core of the defect grows and forms a complete vertical domain: (a) the direct-growth pathway at $h_c = 0.64D_b$ and $\chi N = 12.5$; (b) the top-bridge pathway at $h_c = 0.85D_b$ and $\chi N = 18$; and (c) the middle-bridge pathway at $h_c = 1.22D_b$ and $\chi N = 19$. The red lines in the inset morphologies mark the nascent bridge structures in (a) and the bridges in (b) and (c).

at $\alpha = 0.26$. After the complete formation of the bridge, the edge dislocation is transformed into a disclination with $s = +1/2$ at $\alpha = 0.54$. The following removal process is similar to the removal of the disclination in the top-bridge pathway.

Figure 10 shows the phase-diagram-like map of possible removal pathways of the cross-sectional edge dislocation in the

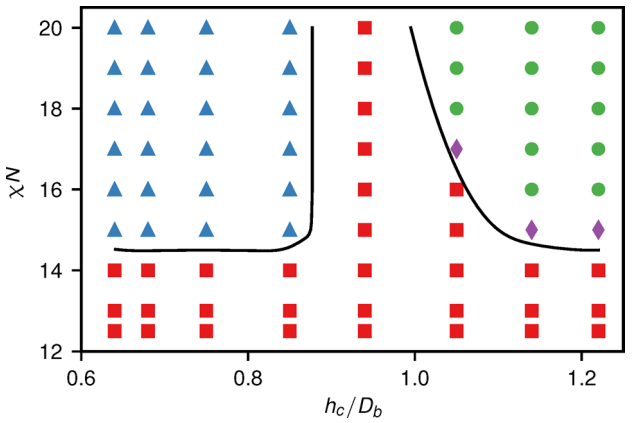

Figure 10. Possible removal pathways of the cross-sectional edge dislocation in the $\chi N \sim h_c$ plane when its core grows to form a complete vertical domain. Red squares: the direct growth pathway; blue up triangles: the top-bridge pathway; green circles: the middle-bridge pathway; and violet diamonds: the transfer growth pathway. The thin film thickness is $2D_b$.

$\chi N \sim h_c$ plane when its core grows to form a complete vertical domain. In contrast to the map in Figure 8, the map is divided in the upper part where the upper left part and the upper right part correspond to the top-bridge pathway and the middle-bridge pathway, respectively. The lower part is occupied by the direct growth pathway where it is not necessary to create any bridge in such weak segregation regime and the difference in the hopping diffusion and the interface diffusion is negligible. In addition, the violet diamonds on the boundary of the region of the direct growth pathway and the region of the middle-bridge pathway correspond to another pathway which is the same as the transfer pathway in Figure 8, except that the height of the core of the edge dislocation increases during the removal process (the MEP is not shown).

4. CONCLUSIONS

Possible removal pathways of two typical out-of-plane defects, the tilted domain defect and the cross-sectional edge dislocation in the thin films of the lamellar-forming diblock copolymers, have been studied extensively. For the tilted domain defect, the removal process can be considered as an order−order transition which follows the nucleation and growth mechanism. The MEP of the removal process consists of multiple free energy barriers, among which the first also the largest one corresponds to the nucleation step. The nucleation starts with a random breakage of a tilted domain, followed by the formation of a bridge which connects the partial domain and its adjacent same component domain. The critical nucleus is composed of a pair of edge dislocations with different component cores, where a new AB interface without any lateral skew emerges. Other energy barriers correspond to the formation of bridges which transfers an A core edge dislocation to a B core edge dislocation or vice versa. A sequence of this transfer process pushes the pair of edge dislocation apart and straight domains form in between, leading to the formation of the defect-free lamellae eventually. We also observed that the number of nucleation events is equal to the number of lamellar periods the tilted domain skews, and their associated energy barriers are approximately the same. In between those energy barriers, there are metastable states corresponding to the dislocation dipoles separated by zero, one, or more straight domains or other more complex defective structures, which are observed in previous experimental works. It implies that the removal of the tilted domain defect is one of the sources for creating other out-of-plane defects. In addition, our observations also suggest that the interaction between two dislocations in a dipole is not necessary always being attractive but can become repulsive by tuning its topological structure.

For the cross-section edge dislocation, the core of the dislocation (a partial vertical domain) can either shrink or grow during the removal process. Multiple removal pathways are revealed by constructing the MEP of the removal process for both cases. For the case of the shrinking of the core, the

DOI: 10.1021/acs.macromol.8b00349
Macromolecules XXXX, XXX, XXX−XXX

evaporation pathway and the breaking pathway occur at small and large h in the weak segregation regime, respectively, while the transfer pathway happens in the relatively strong segregation regime. For the case of the growth of the core, the direct growth pathway is mostly found in the weak segregation regime, while the top-bridge and middle-bridge pathways appear at small and large h_c in the strong segregation regime, respectively. In the strong segregation regime, bridge structures is commonly observed in various removal pathways. We believe it is the most significant feature of all removal pathways that occur in the strong segregation regime. Although the formation of the bridge requires surmounting a free energy barrier, it converts the slow hopping diffusion of polymer chains to the fast interface diffusion. The difference of the rate between these two diffusion modes may exceed an order of magnitude in the strong segregation regime and expands significantly as χN increases, as reported by other theoretical[29,31,32] and experimental[34,45,46] works. In contrast to the strong segregation, only nascent bridge structures that will never develop into actual bridges are observed in the weak segregation regime. The main reason is that the difference between the hopping diffusion and the interface diffusion becomes negligible when χN is low enough.

The ability to produce defect-free structures is essential for the directed self-assembly (DSA) technique becoming an practical tool in industry. We hope our present studies on the removal pathways of out-of-plane defects will shed some new lights on understanding the underlying mechanism of the defect removal process in thin films and developing new strategies to reduce the density of defectivity.

AUTHOR INFORMATION

Corresponding Author

*E-mail: lyx@fudan.edu.cn (Y.-X.L.).

ORCID

Yi-Xin Liu: 0000-0001-9374-5981

Notes

The authors declare no competing financial interest.

ACKNOWLEDGMENTS

This work is supported by the National Natural Science Foundation of China (Grant No. 21004013) and the National Basic Research Program of China (Grant No. 2011CB605701).

REFERENCES

(1) Matsen, M. W.; Schick, M. Stable and unstable phases of a diblock copolymer melt. *Phys. Rev. Lett.* **1994**, *72*, 2660−2663.

(2) Matsen, M. W.; Bates, F. S. Origins of complex self-assembly in block copolymers. *Macromolecules* **1996**, *29*, 7641−7644.

(3) Drolet, F.; Fredrickson, G. H. Combinatorial Screening of Complex Block Copolymer Assembly with Self-Consistent Field Theory. *Phys. Rev. Lett.* **1999**, *83*, 4317−4320.

(4) Tyler, C. A.; Morse, D. C. Orthorhombic Fddd network in triblock and diblock copolymer melts. *Phys. Rev. Lett.* **2005**, *94*, 208302.

(5) Fredrickson, G. H. *The Equilibrium Theory of Inhomogeneous Polymers*; Clarendon Press: Oxford, 2006.

(6) Bates, F. S.; Hillmyer, M. A.; Lodge, T. P.; Bates, C. M.; Delaney, K. T.; Fredrickson, G. H. Multiblock polymers: panacea or Pandora's box? *Science* **2012**, *336*, 434−440.

(7) Arora, A.; Qin, J.; Morse, D. C.; Delaney, K. T.; Fredrickson, G. H.; Bates, F. S.; Dorfman, K. D. Broadly Accessible Self-Consistent Field Theory for Block Polymer Materials Discovery. *Macromolecules* **2016**, *49*, 4675−4690.

(8) Shi, A. C.; Li, B. H. Self-assembly of diblock copolymers under confinement. *Soft Matter* **2013**, *9*, 1398−1413.

(9) Yabu, H.; Higuchi, T.; Jinnai, H. Frustrated phases: polymeric self-assemblies in a 3D confinement. *Soft Matter* **2014**, *10*, 2919−2931.

(10) Kim, H. C.; Park, S. M.; Hinsberg, W. D. Block copolymer based nanostructures: materials, processes, and applications to electronics. *Chem. Rev.* **2010**, *110*, 146−177.

(11) Black, C. T.; Guarini, K. W.; Milkove, K. R.; Baker, S. M.; Russell, T. P.; Tuominen, M. T. Integration of self-assembled diblock copolymers for semiconductor capacitor fabrication. *Appl. Phys. Lett.* **2001**, *79*, 409−411.

(12) Bang, J.; Jeong, U.; Ryu, D. Y.; Russell, T. P.; Hawker, C. J. Block copolymer nanolithography: translation of molecular level control to nanoscale patterns. *Adv. Mater.* **2009**, *21*, 4769−4792.

(13) Tseng, Y. C.; Darling, S. B. Block copolymer nanostructures for technology. *Polymers* **2010**, *2*, 470−489.

(14) Lee, Y.; Gomez, E. D. Challenges and opportunities in the development of conjugated block copolymers for photovoltaics. *Macromolecules* **2015**, *48*, 7385−7395.

(15) Yin, J.; Yao, X. P.; Liou, J. Y.; Sun, W.; Sun, Y. S.; Wang, Y. Membranes with highly ordered straight nanopores by selective swelling of fast perpendicularly aligned block copolymers. *ACS Nano* **2013**, *7*, 9961−9974.

(16) Ji, S. X.; Liu, C. C.; Liu, G. L.; Nealey, P. F. Molecular transfer printing using block copolymers. *ACS Nano* **2010**, *4*, 599−609.

(17) Turner, M. S. Equilibrium properties of a diblock copolymer lamellar phase confined between flat plates. *Phys. Rev. Lett.* **1992**, *69*, 1788−1791.

(18) Walton, D. G.; Kellogg, G. J.; Mayes, A. M.; Lambooy, P.; Russell, T. P. A free-energy model for confined diblock copolymers. *Macromolecules* **1994**, *27*, 6225−6228.

(19) Han, E.; Stuen, K. O.; La, Y. H.; Nealey, P. F.; Gopalan, P. Effect of composition of substrate-modifying random copolymers on the orientation of symmetric and asymmetric diblock copolymer domains. *Macromolecules* **2008**, *41*, 9090−9097.

(20) Trombly, D. M.; Pryamitsyn, V.; Ganesan, V. Surface energies and self-assembly of block copolymers on grafted surfaces. *Phys. Rev. Lett.* **2011**, *107*, 148304.

(21) Liu, C. C.; Ramirez-Hernandez, A.; Han, E.; Craig, G. S. W.; Tada, Y.; Yoshida, H.; Kang, H.; Ji, S.; Gopalan, P.; de Pablo, J. J.; Nealey, P. F. Chemical patterns for directed self-assembly of lamellae-forming block copolymers with density multiplication of features. *Macromolecules* **2013**, *46*, 1415−1424.

(22) Ginzburg, V. V.; Weinhold, J. D.; Hustad, P. D.; Trefonas, P., III Modeling chemoepitaxy of block copolymer thin films using self-consistent field theory. *J. Photopolym. Sci. Technol.* **2013**, *26*, 817−823.

(23) Stoykovich, M. P.; Müller, M.; Kim, S. O.; Solak, H. H.; Edwards, E. W.; de Pablo, J. J.; Nealey, P. F. Directed assembly of block copolymer blends into nonregular device-oriented structures. *Science* **2005**, *308*, 1442−1446.

(24) Bai, W. B.; Gadelrab, K.; Alexander-Katz, A.; Ross, C. A. Perpendicular block copolymer microdomains in high aspect ratio templates. *Nano Lett.* **2015**, *15*, 6901−6908.

(25) Park, S. M.; Stoykovich, M. P.; Ruiz, R.; Zhang, Y.; Black, C. T.; Nealey, P. F. Directed assembly of lamellae-forming block copolymers by using chemically and topographically patterned substrates. *Adv. Mater.* **2007**, *19*, 607−611.

(26) Kim, S. O.; Kim, B. H.; Kim, K.; Koo, C. M.; Stoykovich, M. P.; Nealey, P. F.; Solak, H. H. Defect structure in thin films of a lamellar block copolymer self-assembled on neutral homogeneous and chemically nanopatterned surfaces. *Macromolecules* **2006**, *39*, 5466−5470.

(27) Mahadevapuram, N.; Mitra, I.; Bozhchenko, A.; Strzalka, J.; Stein, G. E. In-plane and out-of-plane defectivity in thin films of lamellar block copolymers. *J. Polym. Sci., Part B: Polym. Phys.* **2016**, *54*, 339−352.

(28) Takahashi, H.; Laachi, N.; Delaney, K. T.; Hur, S. M.; Weinheimer, C. J.; Shykind, D.; Fredrickson, G. H. Defectivity in

DOI: 10.1021/acs.macromol.8b00349
Macromolecules XXXX, XXX, XXX−XXX

laterally confined lamella-forming diblock copolymers: thermodynamic and kinetic aspects. *Macromolecules* **2012**, *45*, 6253−6265.
(29) Hur, S. M.; Thapar, V.; Ramirez-Hernandez, A.; Khaira, G.; Segal-Peretz, T.; Rincon-Delgadillo, P. A.; Li, W. H.; Müller, M.; Nealey, P. F.; de Pablo, J. J. Molecular pathways for defect annihilation in directed self-assembly. *Proc. Natl. Acad. Sci. U. S. A.* **2015**, *112*, 14144−14149.
(30) Nagpal, U.; Müller, M.; Nealey, P. F.; de Pablo, J. J. Free energy of defects in ordered assemblies of block copolymer domains. *ACS Macro Lett.* **2012**, *1*, 418−422.
(31) Li, W. H.; Nealey, P. F.; de Pablo, J. J.; Müller, M. Defect removal in the course of directed self-assembly is facilitated in the vicinity of the order-disorder transition. *Phys. Rev. Lett.* **2014**, *113*, 168301.
(32) Li, W. H.; Müller, M. Thermodynamics and kinetics of defect motion and annihilation in the self-assembly of lamellar diblock copolymers. *Macromolecules* **2016**, *49*, 6126−6138.
(33) Man, X. K.; Zhou, P.; Tang, J. Z.; Yan, D. D.; Andelman, D. Defect-Free Perpendicular Diblock Copolymer Films: The Synergy Effect of Surface Topography and Chemistry. *Macromolecules* **2016**, *49*, 8241−8248.
(34) Tong, Q. Q.; Sibener, S. J. Visualization of individual defect mobility and annihilation within cylinder-forming diblock copolymer thin films on nanopatterned substrates. *Macromolecules* **2013**, *46*, 8538−8544.
(35) Kim, B. H.; Park, S. J.; Jin, H. M.; Kim, J. Y.; Son, S.-W.; Kim, M. H.; Koo, C. M.; Shin, J.; Kim, J. U.; Kim, S. O. Anomalous Rapid Defect Annihilation in Self-Assembled Nanopatterns by Defect Melting. *Nano Lett.* **2015**, *15*, 1190−1196.
(36) Ruiz, R.; Kang, H.; Detcheverry, F. A.; Dobisz, E.; Kercher, D. S.; Albrecht, T. R.; de Pablo, J. J.; Nealey, P. F. Density multiplication and improved lithography by directed block copolymer assembly. *Science* **2008**, *321*, 936−939.
(37) Bita, I.; Yang, J. K. W.; Jung, Y. S.; Ross, C. A.; Thomas, E. L.; Berggren, K. K. Graphoepitaxy of self-assembled block copolymers on two-dimensional periodic patterned templates. *Science* **2008**, *321*, 939−943.
(38) Li, W. H.; Müller, M. Defects in the self-assembly of block copolymers and their relevance for directed self-assembly. *Annu. Rev. Chem. Biomol. Eng.* **2015**, *6*, 187−216.
(39) Lodge, T. P.; Dalvi, M. C. Mechanisms of chain diffusion in lamellar block-copolymers. *Phys. Rev. Lett.* **1995**, *75*, 657−660.
(40) Lodge, T. P.; Hamersky, M. W.; Milhaupt, J. M.; Kannan, R. M.; Dalvi, M. C.; Eastman, C. E. Diffusion in microstructured block copolymer melts. *Macromol. Symp.* **1997**, *121*, 219−233.
(41) Dalvi, M. C.; Lodge, T. P. Parallel and perpendicular chain diffusion in a lamellar block copolymer. *Macromolecules* **1993**, *26*, 859−861.
(42) Ehlich, D.; Takenaka, M.; Okamoto, S.; Hashimoto, T. FRS study of the diffusion of a block copolymer 0.1. direct determination of the anisotropic diffusion of block copolymer chains in a lamellar microdomain. *Macromolecules* **1993**, *26*, 189−197.
(43) Fleischer, G.; Rittig, F.; Stepanek, P.; Almdal, K.; Papadakis, C. M. Self-diffusion of a symmetric PEP-PDMS diblock copolymer above and below the disorder-to-order transition. *Macromolecules* **1999**, *32*, 1956−1961.
(44) Hamersky, M. W.; Tirrell, M.; Lodge, T. P. Anisotropy of diffusion in a lamellar styrene-isoprene block copolymer. *Langmuir* **1998**, *14*, 6974−6979.
(45) Cavicchi, K. A.; Lodge, T. P. Anisotropic self-diffusion in block copolymer cylinders. *Macromolecules* **2004**, *37*, 6004−6012.
(46) Rittig, F.; Fleischer, G.; Karger, J.; Papadakis, C. M.; Almdal, K.; Stepanek, P. Anisotropic self-diffusion in a hexagonally ordered asymmetric PEP-PDMS diblock copolymer studied by pulsed field gradient NMR. *Macromolecules* **1999**, *32*, 5872−5877.
(47) Tsarkova, L.; Knoll, A.; Magerle, R. Rapid transitions between defect configurations in a block copolymer melt. *Nano Lett.* **2006**, *6*, 1574−1577.
(48) Yokoyama, H. Diffusion of block copolymers. *Mater. Sci. Eng., R* **2006**, *53*, 199−248.
(49) Hamersky, M. W.; Hillmyer, M. A.; Tirrell, M.; Bates, F. S.; Lodge, T. P.; von Meerwall, E. D. Block copolymer self-diffusion in the gyroid and cylinder morphologies. *Macromolecules* **1998**, *31*, 5363−5370.
(50) Segal-Peretz, T.; Winterstein, J.; Doxastakis, M.; Ramirez-Hernandez, A.; Biswas, M.; Ren, J.; Suh, H. S.; Darling, S. B.; Liddle, J. A.; Elam, J. W.; de Pablo, J. J.; Zaluzec, N. J.; Nealey, P. F. Characterizing the three-dimensional structure of block copolymers via sequential infiltration synthesis and scanning transmission electron tomography. *ACS Nano* **2015**, *9*, 5333−5347.
(51) Stein, G. E.; Mahadevapuram, N.; Mitra, I. Controlling interfacial interactions for directed self assembly of block copolymers. *J. Polym. Sci., Part B: Polym. Phys.* **2015**, *53*, 96−102.
(52) Tsori, Y.; Andelman, D. Surface induced ordering in thin film diblock copolymers: tilted lamellar phases. *J. Chem. Phys.* **2001**, *115*, 1970−1978.
(53) Chen, P.; Liang, H. J.; Xia, R.; Qian, J. S.; Feng, X. S. Directed self-assembly of block copolymers on sparsely nanopatterned substrates. *Macromolecules* **2013**, *46*, 922−926.
(54) Mitra, I.; Mahadevapuram, N.; Strzalka, J.; Stein, G. E. Tilting of lamellar domains on neutral random copolymer brushes. *Proc. SPIE* **2015**, *9423*, 942320.
(55) Bosworth, J. K.; Dobisz, E. A.; Hellwig, O.; Ruiz, R. Impact of out-of-plane translational order in block copolymer lithography. *Macromolecules* **2011**, *44*, 9196−9204.
(56) Vu, T.; Mahadevapuram, N.; Perera, G. M.; Stein, G. E. Controlling Domain Orientations in Thin Films of AB and ABA Block Copolymers. *Macromolecules* **2011**, *44*, 6121−6127.
(57) Hur, S. M.; Khaira, G. S.; Ramirez-Hernandez, A.; Müller, M.; Nealey, P. F.; de Pablo, J. J. Simulation of defect reduction in block copolymer thin films by solvent annealing. *ACS Macro Lett.* **2015**, *4*, 11−15.
(58) Lo, T. Y.; Dehghan, A.; Georgopanos, P.; Avgeropoulos, A.; Shi, A. C.; Ho, R. M. Orienting block copolymer thin films via entropy. *Macromolecules* **2016**, *49*, 624−633.
(59) Sun, Z.; Russell, T. P. In situ grazing incidence small-angle X-ray scattering study of solvent vapor annealing in lamellae-forming block copolymer thin films: Trade-off of defects in deswelling. *J. Polym. Sci., Part B: Polym. Phys.* **2017**, *55*, 980−989.
(60) Sivaniah, E.; Hayashi, Y.; Iino, M.; Hashimoto, T.; Fukunaga, K. Observation of perpendicular orientation in symmetric diblock copolymer thin films on rough substrates. *Macromolecules* **2003**, *36*, 5894−5896.
(61) Sivaniah, E.; Hayashi, Y.; Matsubara, S.; Kiyono, S.; Hashimoto, T.; Fukunaga, K.; Kramer, E.; Mates, T. Symmetric diblock copolymer thin films on rough substrates. Kinetics and structure formation in pure block copolymer thin films. *Macromolecules* **2005**, *38*, 1837−1849.
(62) E, W. N.; Ren, W. Q.; Vanden-Eijnden, E. String method for the study of rare events. *Phys. Rev. B: Condens. Matter Mater. Phys.* **2002**, *66*, 052301.
(63) E, W. N.; Ren, W. Q.; Vanden-Eijnden, E. Simplified and improved string method for computing the minimum energy paths in barrier-crossing events. *J. Chem. Phys.* **2007**, *126*, 164103.
(64) Cheng, X. Y.; Lin, L.; E, W. N.; Zhang, P. W.; Shi, A. C. Nucleation of ordered phases in block copolymers. *Phys. Rev. Lett.* **2010**, *104*, 148301.
(65) Ji, N.; Tang, P.; Qiu, F.; Shi, A.-C. Kinetic pathways of lamellae to gyroid transition in weakly segregated diblock copolymers. *Macromolecules* **2015**, *48*, 8681−8693.
(66) Helfand, E. Theory of inhomogeneous polymers: fundamentals of the gaussian random-walk model. *J. Chem. Phys.* **1975**, *62*, 999−1005.
(67) Chantawansri, T. L.; Hur, S. M.; Garcia-Cervera, C. J.; Ceniceros, H. D.; Fredrickson, G. H. Spectral collocation methods for polymer brushes. *J. Chem. Phys.* **2011**, *134*, 244905.

DOI: 10.1021/acs.macromol.8b00349
Macromolecules XXXX, XXX, XXX−XXX

(68) Liu, Y. X.; Zhang, H. D. Exponential time differencing methods with Chebyshev collocation for polymers confined by interacting surfaces. *J. Chem. Phys.* **2014**, *140*, 224101.
(69) Matsen, M. W. Thin films of block copolymer. *J. Chem. Phys.* **1997**, *106*, 7781−7791.
(70) Welander, A. M.; Kang, H.; Stuen, K. O.; Solak, H. H.; Müller, M.; de Pablo, J. J.; Nealey, P. F. Rapid directed assembly of block copolymer films at elevated temperatures. *Macromolecules* **2008**, *41*, 2759−2761.
(71) Lin, L.; Cheng, X.; E, W.; Shi, A.-C.; Zhang, P. A numerical method for the study of nucleation of ordered phases. *J. Comput. Phys.* **2010**, *229*, 1797−1809.
(72) Zhang, X. H.; Berry, B. C.; Yager, K. G.; Kim, S.; Jones, R. L.; Satija, S.; Pickel, D. L.; Douglas, J. F.; Karim, A. Surface morphology diagram for cylinder-forming block copolymer thin films. *ACS Nano* **2008**, *2*, 2331−2341.
(73) Son, J. G.; Bulliard, X.; Kang, H.; Nealey, P. F.; Char, K. Surfactant-assisted orientation of thin diblock copolymer films. *Adv. Mater.* **2008**, *20*, 3643−3648.
(74) Han, E.; Stuen, K. O.; Leolukman, M.; Liu, C. C.; Nealey, P. F.; Gopalan, P. Perpendicular orientation of domains in cylinder-forming block copolymer thick films by controlled interfacial interactions. *Macromolecules* **2009**, *42*, 4896−4901.
(75) Bates, C. M.; Maher, M. J.; Janes, D. W.; Ellison, C. J.; Willson, C. G. Block copolymer lithography. *Macromolecules* **2014**, *47*, 2−12.
(76) Kim, B.; Laachi, N.; Delaney, K. T.; Carilli, M.; Kramer, E. J.; Fredrickson, G. H. Thermodynamic and kinetic aspects of defectivity in directed self-assembly of cylinder-forming diblock copolymers in laterally confining thin channels. *J. Appl. Polym. Sci.* **2014**, *131*, 40790.
(77) Chandrasekhar, S. *Liquid Crystals*, 2nd ed.; Cambridge University Press: Cambridge, 1992.

DOI: 10.1021/acs.macromol.8b00349
Macromolecules XXXX, XXX, XXX−XXX